

Solution-Grown Silver Nanowire Ordered Arrays as Transparent Electrodes

Beniamino Sciacca, Jorik van de Groep, Albert Polman, and Erik C. Garnett*

Transparent conductors are crucial components in optoelectronic devices, such as touch screen displays, organic light emitting diodes, and solar cells.^[1,2] Transparent conducting oxides are the most commonly used in these applications, with indium-tin-oxide (ITO) leading the market.^[3] However, the costly deposition process of ITO and the incompatibility with flexible electronics, due to the brittleness of thick films,^[4,5] have triggered intensive research toward alternative schemes that can simultaneously provide high electrical conductivity, high optical transmittance, and flexibility. Materials that have recently been investigated include carbon nanotubes,^[4,6–8] conducting polymers,^[4,9,10] percolated metal films,^[11–13] graphene,^[4,14,15] and metal nanowire networks.^[4,16–24]

Metal nanowire networks composed of, e.g., Ag, Cu, and Al have proven to be excellent transparent conductors.^[16–18,22,23,25] The bulk conductivity of these metals is high, and nanostructured wires effectively couple light into an underlying substrate through the excitation and scattering of plasmons.^[16,17,23,24] Several approaches to realize metal nanowire networks with high transmittance and low sheet resistance that can be made at low costs have been explored so far. These include nanowire meshes prepared by metal evaporation on various templates, such as electrospun fibers,^[22,26,27] self-cracking templates,^[19] or lithography-defined nanopatterns.^[16,17] Such approaches typically require thermal evaporation in order to deposit metal. Although vacuum processes allow to deposit high quality materials, they are energy intensive, time consuming, and make inefficient use of metal. Cost-effective alternatives based on deposition and welding of metal nanowires prepared in solution have proven effective to achieve transparent electrodes with remarkable performance.^[5,21,24,28,29] This shows that solution processes can yield material of similar quality compared to vacuum-based methods. Although this method provides a relatively simple fabrication scheme, the random geometry limits control over the optical transmission characteristics, which are determined by the subtle interplay between plasmons on the interacting nanowires. To achieve such control, ordered arrays of nanowires have been made by lithographic techniques.^[16,17,30] Using these arrays, accurate control over the excited plasmon modes and their interaction, via tuning of the nanowire width, height, and pitch of the array, has led to performance beyond that of ITO.^[17] Furthermore,

it has been shown that the accurate design of patterns at the nanoscale (such as fractal geometries), can yield electrodes with superior optoelectronic performance.^[31] In fact, this enables (i) minimum sheet resistance (for a certain transmittance) via tuning of the geometry, (ii) coupling to specific optical modes, and (iii) light trapping or directional emission. As such optimal features are only achievable with an engineered pattern, the successful integration of nanopatterning with solution processing techniques would be an important step toward replacing expensive metal oxide films as transparent electrodes.

Here, we demonstrate a strategy that bridges the gap between the efficiency of solution phase processes, and the control of light-matter interaction at the nanoscale using nanopatterning. We combine substrate-conformal imprint-lithography (SCIL) with a soft solution process to fabricate highly controlled 2D networks of silver nanowires without metal evaporation steps. First, SCIL is used to make a square array of trenches in a poly(methyl methacrylate) (PMMA) film that is spin-coated on glass (trench width 50–130 nm, pitch 300–1000 nm). Second, the reduction of a silver salt (AgNO_3) by a sugar (glucose) in an aqueous solution is used to locally infill the trenches with silver, following a chemical route commonly employed as a simple test for the presence of aldehydes (Tollens' test). Using this method, we obtain a solution-grown nanowire network on glass with a well-controlled geometry. We find that the electrical performance outperforms that of evaporated networks with an almost three-fold decrease in resistivity ($3.5 \Omega \text{ sq}^{-1}$ vs $10.7 \Omega \text{ sq}^{-1}$ at a transmission of 76%, weighted for AM1.5 photon density). The controlled 2D network allows us to confidently compare different metal deposition pathways and derive conclusions about their performance. Based on detailed characterization and a simple conductivity model, we show that the high conductance of the solution-grown networks can be explained by a large increase in the grain size of silver nanocrystallites within the nanowires, compared to the evaporated wires. This shows that the material quality achievable with solution deposition methods can match or even exceed that obtained with vacuum-based techniques.

The fabrication of solution-grown nanowire networks is summarized in **Figure 1a**. It involves four steps (see the Supporting Information for more details): (i) use of SCIL to imprint nanosized trenches in a PMMA template, organized in a grid fashion; (ii) use of the Tollens' reaction to nucleate and grow crystalline silver on the substrate surface; (iii) lift-off of the PMMA template to obtain a transparent and conductive nanowire network; (iv) use of rapid thermal annealing (RTA) to reduce surface roughness.

Silver was chosen as the material for the solution grown nanowire networks because of its exceptional conductivity and better chemical stability compared to copper. The Tollens'

Dr. B. Sciacca, J. van de Groep,
Prof. A. Polman, Dr. E. C. Garnett
Center for Nanophotonics
FOM Institute AMOLF
Science Park 104, 1098 XG Amsterdam, The Netherlands
E-mail: e.garnett@amolf.nl



DOI: 10.1002/adma.201504045

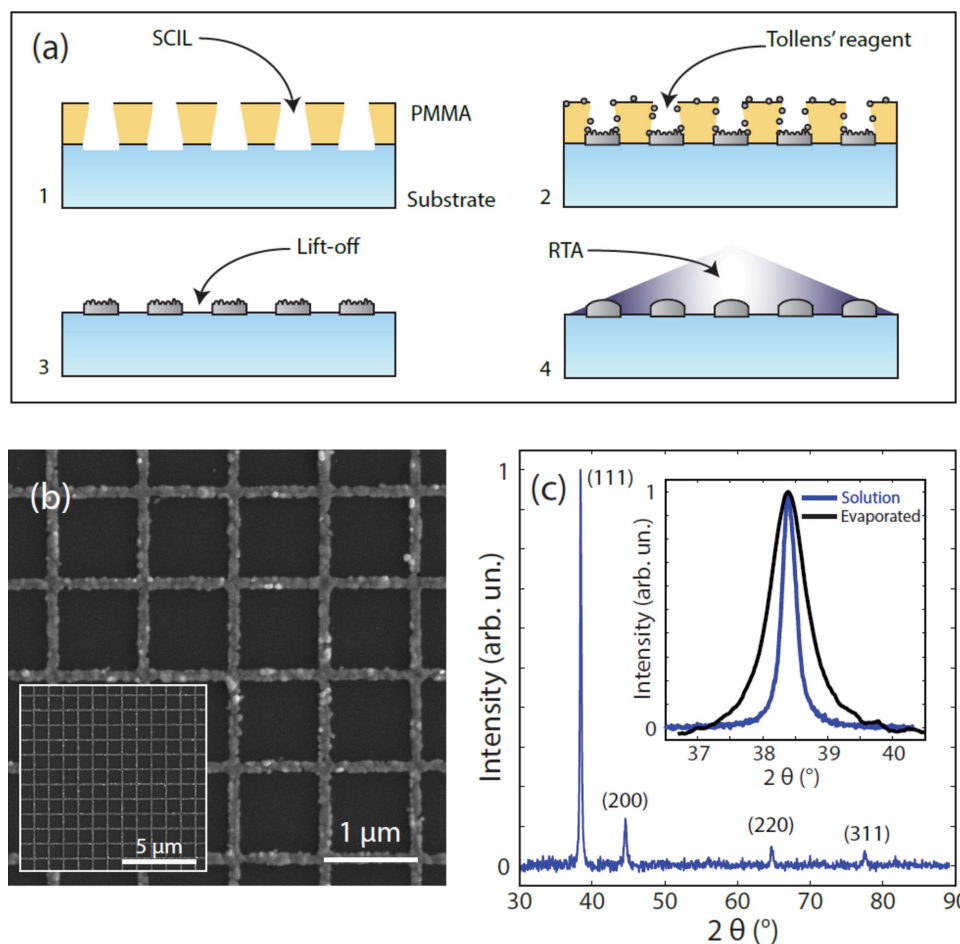
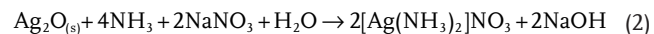
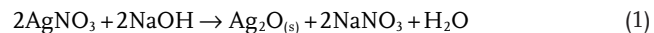


Figure 1. a) Schematic of the solution grown nanowire network fabrication process: (1) SCIL to produce a grid nanopattern in PMMA, (2) solution phase growth of Ag nanowires in the trenches defined by the template via the Tollens' reaction, (3) lift-off, and (4) RTA to smooth the nanowire surface. b) SEM images of a freshly grown nanowire network before RTA treatment, showing the confinement of the growth over a large area. c) XRD before RTA treatment of solution grown nanowire network measured in the range 30° – 90° with the θ – 2θ configuration, showing the crystalline nature of the nanowire; inset: comparison of the (111) Ag reflection peak for solution grown and evaporated silver, indicating the larger average grain size in the former.

reaction,^[32] causes the formation of silver nanocrystals when a sugar with an aldehyde group, such as glucose, is present in a solution containing diamminesilver(I) complexes (see Equation (1)–(3))



Nanocrystals preferentially form at the substrate surface due to the lower nucleation barrier. Some partial nucleation occurs also on the PMMA template surface, at a much lower rate compared to that at the glass substrate. This allows for successful lift-off on the entire sample because the nanowires growing in the trenches and nanoparticles nucleating on the template are physically separated. The SCIL stamp contained several fields with different nanowire width and pitch, each field having a total size of $2 \times 2 \text{ mm}^2$.

Figure 1b shows scanning electron microscope (SEM) images of a solution grown nanowire network after lift-off. The images show the confined growth of silver only on the exposed glass surface, and indicate the continuity of the network over a large area. A dark-field optical image of the network is displayed in Figure S1 (Supporting Information). High-magnification SEM images are shown in Figure S2 (Supporting Information). The surface texture of the silver nanogrid suggests that nucleation takes place at many different positions in the trench on the substrate surface, followed by growth of individual nanocrystals until merging with neighbors. As a result, a continuous network of crystalline silver is formed. The X-ray diffraction (XRD) pattern presented in Figure 1c shows the characteristic reflection peaks of crystalline silver with no secondary phases.

The average Ag grain size for the solution-grown nanowires, estimated from the X-ray diffraction peak width using the Scherrer equation (see the Supporting Information), is $\approx 60 \text{ nm}$ (inset in Figure 1c). X-ray diffraction peak width measurements were also performed on silver evaporated using the method described in ref. [16], and show a silver grain size of $\approx 15 \text{ nm}$.

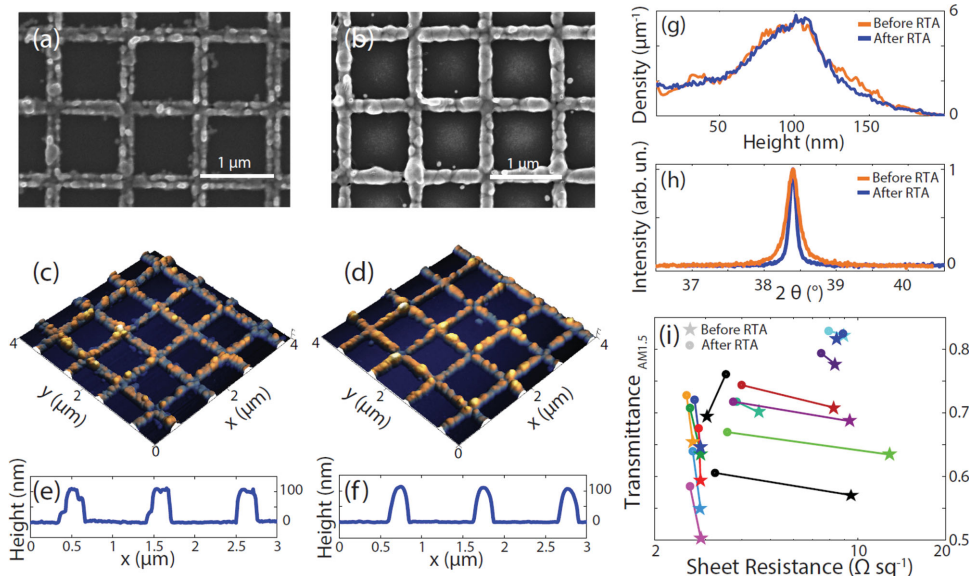


Figure 2. a–d) SEM and AFM images of solution grown nanowire networks samples a,c) before and b,d) after RTA; the aspect ratio of AFM images is 1. e,f) Cross-cuts of the AFM map of (c) and (d), respectively. g) Probability density function of the height distribution computed from (c) and (d), showing a slightly narrower peak after RTA annealing, as a result of smoothing and homogenization of the nanowires. h) XRD of solution grown nanowire networks before and after RTA, showing a narrower (111) silver reflection peak as a result of the larger average grain size due to RTA. i) Evolution of the optical /electrical performance of solution grown nanowire networks of various height, as a result of RTA; star and circle markers indicate the sample before and after RTA, respectively.

Clearly, the solution-growth method leads to larger Ag grains and thus a smaller density of grain boundaries.

The surface topography of the solution-grown silver nanowire networks was characterized by atomic force microscopy (AFM) on a $100 \mu\text{m}^2$ area (Figure S3a, Supporting Information). The average height across a Ag nanowire network is shown in Figure S3b (Supporting Information), indicating for this particular sample a typical nanowire height of 30–40 nm. The nanowire height can be controlled by adjusting the growth time.

Because of the formation process, i.e., random nucleation and growth, the surface of as grown nanowire networks is rough. This causes strong scattering and absorption of light, which limits optical transmittance and therefore reduces performance. It has been shown that solution synthesized silver nanowires can be plasmonically welded by RTA,^[18] at temperatures below the melting point of silver, preserving the nanowire shape. High intensity broad-band light is absorbed by the metal nanowires, causing heating; silver atoms become highly mobile well below the melting point,^[18] and diffuse to minimize the surface to volume ratio. Furthermore, the electromagnetic field can be locally enhanced due to roughness, resulting in hot spots that create additional heating where the surface is rougher. This effectively contributes to the reduction of the surface to volume ratio, therefore leading to a smoother surface. Following this paradigm we performed RTA on solution grown nanowire.

Figure 2a–d compares SEM and AFM images of solution grown nanowire networks before and after 7 s of RTA. The difference in surface texture observed in the figure, indicates a smoothing of the nanowires as a result of RTA. Cross-cuts of AFM data show that indeed after RTA, the nanowires display a rounded cross-section compared to as grown nanowires

(Figure 2e,f), and become smoother. Statistical analysis of the entire AFM scan was performed, by computing the probability density function of the nanowire height distribution. This allows us to investigate trends representative of a larger area. Figure 2g compares the height distribution of the nanowires before (orange) and after (blue) RTA. It shows that after RTA the distribution is slightly narrower, indicating that the nanowires become more uniform in height. Figure 2h compares XRD data of the (111) silver peak before (orange) and after RTA (blue). It shows that a narrower peak is obtained after RTA, corresponding to an average grain size of ≈ 200 nm, calculated using the Scherrer equation. Considering the relatively low temperature achieved during the process,^[18] which is expected to be well below the melting point (T_{mp}) of silver, we exclude melting of the nanowires followed by solidification to achieve recrystallization with larger grains. This increase in average grain size can however be explained in terms of gain of interfacial free energy as a result of grain boundary migration, which has been reported to occur at temperatures as small as $0.2 T_{\text{mp}}$ in metals.^[33]

We next characterized electrical and optical response of RTA-processed solution-grown nanowire networks. This is presented in Figure 2i, which compares performance before RTA (star) and after RTA (circle), for networks of various height, pitch and width. The performance of the networks improves upon RTA processing, independent of the array geometry. The transmittance (T) of the network improves significantly, up to 10% absolute. Furthermore, an improvement of sheet resistance (R_{sh}) is observed as well in almost every sample, due to the enlargement of the average grain size and the concurrent homogenization of the nanowire height distribution.

Having demonstrated the efficacy of RTA to improve the performance of solution grown nanowire networks, we summarize

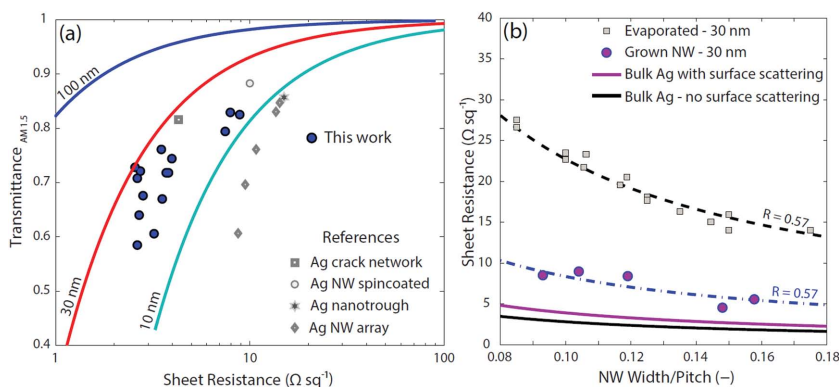


Figure 3. a) Optical versus electrical performance of solution grown nanowire networks, represented by blue solid markers, for different nanowire width, height, and pitch of the array. The performance of Ag nanowire array,^[14] Ag nanotrough,^[20] Ag crack network,^[17] Ag nanowire spincoated,^[19] is reported for comparison after weighting for the AM 1.5 spectrum; solid lines represent the performance of ideal nanowire grids of different thicknesses. b) Sheet resistance of 30 nm thin nanowire grids as a function of nanowire width/pitch, according to the Mayadas–Shatzkes model described in Equation (S2f) (Supporting Information), that accounts for electron scattering at the surface and by grain boundaries, with a $p = 0.5$ specularity parameter and $R = 0.57$ reflection coefficient; the average grain size employed in the model was calculated from XRD measurements and corresponds to 15 nm for evaporated (black dashed line) and 60 nm for solution grown nanowire networks (blue dashed line); the solid curve represent the sheet resistance of a defect-free nanowire grid, accounting for surface scattering ($p = 0.5$, magenta curve) and assuming values for bulk materials ($p = 1$, black curve); data points represent measured sheet resistance of solution-grown (magenta dots) and of evaporated nanowire networks (gray squares) with a thickness of 30 nm; the smaller sheet resistance measured for solution-grown networks compared to evaporated networks is due to the larger average grain size in the former (60 nm vs 15 nm); this is accurately described by the Mayadas–Shatzkes model.

in **Figure 3a** optical transmission and sheet resistance measurements of best performing samples. The solid blue points represent solution-grown nanowire networks with different nanowire widths in the range 90–180 nm, periodicities of 800, 900, and 1000 nm, and heights in the range 30–100 nm. The transmittance data were calculated by weighting the transmission spectra over the photon density in the AM1.5 spectrum (see **Figure S4**, Supporting Information, for transmission spectra), and normalized to the transmission of a bare, flat substrate (see **Figure S5**, Supporting Information, for an example of a haze measurement). We note that the transmittance derived this way is underestimated, as this analysis does not take into account light coupled into guided modes in the substrate (see ref. [16]); such scattered and trapped light does contribute to power generation in a photovoltaic device. The sheet resistance was obtained from four-point-probe measurements.

As reference, the lines drawn in **Figure 3a** represent the calculated performance for defect-free metal nanowire grids of three different thicknesses based on a simple geometrical transmission model. The curves are obtained by varying the nanowire width to pitch ratio. The calculated transmittance accounts for both transmission through the voids and transmission through the metal (this is important for thin films). The transmittance is weighted for the AM1.5 spectrum. While no plasmonic effects are included in the calculation, this simple model accurately represents experimental transmittance data (see **Figure S6** in the Supporting Information), which we attribute to the fact that the relatively narrow resonances only have a small effect on the average broadband response. The

sheet resistance accounts for electron scattering at the surface but assumes no grain boundaries, and was calculated by employing the Mayadas and Shatzkes model^[34] (see the Supporting Information). The curves show the typical trade-off between T and R_{sh} , which can be accurately controlled by varying pitch, width, and thickness of the nanowire networks.

Next, the performance of our solution-grown nanowire networks is compared to that of nanowire-based transparent electrodes fabricated in other ways reported in the literature; the data are shown for reference in **Figure 3a**. We find superior performance for the solution-grown networks compared to the same nanowire networks obtained by metal evaporation (gray diamonds).^[16] Ag crack networks are obtained by metal evaporation on a cracked gel film template;^[19] Ag nanotroughs are obtained by metal evaporation on suspended electrospun fibers;^[22] spincoated Ag nanowires are obtained by spincoating Ag nanowires prepared in solution with the polyol process.^[21] This shows that our solution grown nanowire networks have outstanding performance. Note that the values reported for the reference networks were calculated by applying the AM1.5 weighting function to the wavelength dependent trans-

mittance data available in the references. Also, all data in **Figure 3a** are referenced to the transmission of a glass substrate; this results in absolute 8% overestimation of the transmittance.

We chose not to overlay in **Figure 3a** the widely used figure of merit (defined as the ratio between DC conductivity to optical conductivity)^[8,17,19,20,28] because it is not applicable in the optical frequency regime studied here, and it is only true for the limiting case where optical and DC conductivity are equal (see the Supporting Information for a more detailed explanation). Furthermore, the relative performance of transparent electrodes having different geometry, T and R_{sh} strongly depends on the technological application.^[35] Using a single number (or figure of merit) to compare unconditionally transparent electrodes can be highly deceiving, as this number can be made arbitrarily large (see the Supporting Information for a practical example).

In order to understand the superior performance of solution deposited Ag nanowire compared to those made by evaporation, we employed the model developed by Mayadas and Shatzkes,^[34] which describes the relation between conductivity of nanoscale metallic films and electron scattering at grain boundaries and at the surface (see Equation (S2), Supporting Information). The sheet resistance of solution-grown nanowire networks and evaporated networks (both with a thickness of 30 nm) is reported in **Figure 3b** as a function of the ratio between the nanowire width and the pitch of the array, showing the trend that larger filling fractions correspond to smaller sheet resistances. It also shows that for a fixed nanowire width/pitch ratio, the conductivity of solution grown nanowire networks is on average 2.5 times better than that of evaporated networks.

Figure 3b shows the modeled sheet resistance of the grid calculated from Equation (S2f) (Supporting Information), for 60 nm grain size (dashed blue line) and 15 nm grain size (dashed black line), in accordance with the average grain size obtained from XRD data (Figure 1c). The excellent match between the model and experimental data for solution processed and evaporated films, indicates that the larger conductivity of the solution processed wires originates from the larger grain size. Note that the data reported in Figure 3b for solution-grown nanowire networks were measured before RTA processing. Using the same grain boundary and surface scattering model parameters (see the Supporting Information for full description), we could achieve good fits to the experimental data for both solution-grown and evaporated nanowire networks simply by inputting the grain size calculated from XRD. The calculated sheet resistance of the same silver nanowire grid without grain boundary scattering (i.e., monocrystalline Ag) is also given in Figure 3b for comparison, both with and without surface scattering contributions (magenta and black solid lines, respectively). This shows that our solution grown nanowire networks are less than a factor of 2 from the sheet resistance expected from a defect-free grid. Detailed characterization of the nanowire networks thus indicates that solution deposition methods can match or even exceed the material quality of vacuum-based deposition, in stark contrast to the conventional wisdom in the field.

We demonstrate high-quality silver nanowire networks fabricated by a combination of soft-imprint lithography and soft-solution processing (Tollens' reaction). This relatively simple method yields ordered metal nanowire grids as transparent electrodes, without the need for energy intensive vacuum metal evaporation processes. We show that the solution process, combined with a short RTA treatment, yields superior performance compared to the thermally evaporated networks. This important result shows that solution-based methods can lead to material quality comparable or even superior to vacuum-based deposition methods, in contrast with common assumptions. We demonstrate that the lower material resistance is due to the larger average grain size, which decreases electron scattering from grain boundaries. The simplicity of this solution approach can be extended to other types of template-assisted metal nanowire network transparent electrodes, thus providing a general pathway for further improvement of transparent conductor performance at low cost.

Supporting Information

Supporting Information is available from the Wiley Online Library or from the author.

Acknowledgements

The authors gratefully acknowledge Dr. Wim Noorduyn for careful reading of the manuscript, Sander Mann for his help with haze measurements, and Henk-Jan Boluijt for the ToC schematic. The work at AMOLF is part of the research program of the "Stichting voor Fundamenteel Onderzoek der Materie (FOM)," which is financially supported by the "Nederlandse Organisatie voor Wetenschappelijk Onderzoek (NWO)." The research leading to these results received funding from the European Research Council under the European Union's Seventh Framework Programme

(FP/2007–2013)/ERC Grant Agreement no. 337328, "NanoEnabledPV" and no. 267634, "Plasmeta".

Received: August 19, 2015

Revised: September 28, 2015

Published online: December 3, 2015

- [1] K. Ellmer, *Nat. Photonics* **2012**, *6*, 808.
- [2] E. Fortunato, P. Barquinha, R. Martins, *Adv. Mater.* **2012**, *24*, 2945.
- [3] K. Ghaffarzadeh, R. Das, *Transparent Conductive Films (TCF) 2015–2025: Forecasts, Markets, Technologies (IDTechEx)* June, **2015**.
- [4] D. S. Hecht, L. B. Hu, G. Irvin, *Adv. Mater.* **2011**, *23*, 1482.
- [5] S. R. Ye, A. R. Rathmell, Z. F. Chen, I. E. Stewart, B. J. Wiley, *Adv. Mater.* **2014**, *26*, 6670.
- [6] Q. Cao, S. H. Hur, Z. T. Zhu, Y. G. Sun, C. J. Wang, M. A. Meitl, M. Shim, J. A. Rogers, *Adv. Mater.* **2006**, *18*, 304.
- [7] Z. C. Wu, Z. H. Chen, X. Du, J. M. Logan, J. Sippel, M. Nikolou, K. Kamaras, J. R. Reynolds, D. B. Tanner, A. F. Hebard, A. G. Rinzler, *Science* **2004**, *305*, 1273.
- [8] L. Hu, D. S. Hecht, G. Gruner, *Nano Lett.* **2004**, *4*, 2513.
- [9] S. I. Na, S. S. Kim, J. Jo, D. Y. Kim, *Adv. Mater.* **2008**, *20*, 4061.
- [10] A. A. Argun, A. Cirpan, J. R. Reynolds, *Adv. Mater.* **2003**, *15*, 1338.
- [11] K. Tvingstedt, O. Inganas, *Adv. Mater.* **2007**, *19*, 2893.
- [12] T. C. Gao, B. M. Wang, B. Ding, J. K. Lee, P. W. Leu, *Nano Lett.* **2014**, *14*, 3694.
- [13] P. C. Hsu, S. Wang, H. Wu, V. K. Narasimhan, D. Kong, H. R. Lee, Y. Cui, *Nat. Commun.* **2013**, *4*, 2522.
- [14] G. Eda, G. Fanchini, M. Chhowalla, *Nat. Nanotechnol.* **2008**, *3*, 270.
- [15] K. S. Kim, Y. Zhao, H. Jang, S. Y. Lee, J. M. Kim, K. S. Kim, J. H. Ahn, P. Kim, J. Y. Choi, B. H. Hong, *Nature* **2009**, *457*, 706.
- [16] J. van de Groep, D. Gupta, M. A. Verschuuren, M. M. Wienk, R. A. Janssen, A. Polman, *Sci. Rep.* **2015**, *5*, 11414.
- [17] J. V. van de Groep, P. Spinelli, A. Polman, *Nano Lett.* **2012**, *12*, 3138.
- [18] E. C. Garnett, W. S. Cai, J. J. Cha, F. Mahmood, S. T. Connor, M. G. Christoforo, Y. Cui, M. D. McGehee, M. L. Brongersma, *Nat. Mater.* **2012**, *11*, 241.
- [19] B. Han, K. Pei, Y. L. Huang, X. J. Zhang, Q. K. Rong, Q. G. Lin, Y. F. Guo, T. Y. Sun, C. F. Guo, D. Carnahan, M. Giersig, Y. Wang, J. W. Gao, Z. F. Ren, K. Kempa, *Adv. Mater.* **2014**, *26*, 873.
- [20] L. B. Hu, H. Wu, Y. Cui, *MRS Bull.* **2011**, *36*, 760.
- [21] D. S. Leem, A. Edwards, M. Faist, J. Nelson, D. D. C. Bradley, J. C. de Mello, *Adv. Mater.* **2011**, *23*, 4371.
- [22] H. Wu, D. S. Kong, Z. C. Ruan, P. C. Hsu, S. Wang, Z. F. Yu, T. J. Carney, L. B. Hu, S. H. Fan, Y. Cui, *Nat. Nanotechnol.* **2013**, *8*, 421.
- [23] P. B. Catrysse, S. H. Fan, *Nano Lett.* **2010**, *10*, 2944.
- [24] J. Y. Lee, S. T. Connor, Y. Cui, P. Peumans, *Nano Lett.* **2008**, *8*, 689.
- [25] K. Critchley, B. P. Khanal, M. L. Gorzyn, L. Vigderman, S. D. Evans, E. R. Zubarev, N. A. Kotov, *Adv. Mater.* **2010**, *22*, 2338.
- [26] P. C. Hsu, D. S. Kong, S. Wang, H. T. Wang, A. J. Welch, H. Wu, Y. Cui, *J. Am. Chem. Soc.* **2014**, *136*, 10593.
- [27] H. Wu, L. B. Hu, M. W. Rowell, D. S. Kong, J. J. Cha, J. R. McDonough, J. Zhu, Y. A. Yang, M. D. McGehee, Y. Cui, *Nano Lett.* **2010**, *10*, 4242.
- [28] S. De, T. M. Higgins, P. E. Lyons, E. M. Doherty, P. N. Nirmalraj, W. J. Blau, J. J. Boland, J. N. Coleman, *ACS Nano* **2009**, *3*, 1767.
- [29] L. B. Hu, H. S. Kim, J. Y. Lee, P. Peumans, Y. Cui, *ACS Nano* **2010**, *4*, 2955.
- [30] M. G. Kang, L. J. Guo, *Adv. Mater.* **2007**, *19*, 1391.
- [31] F. Afshinmanesh, A. G. Curto, K. M. Milaninia, N. F. van Hulst, M. L. Brongersma, *Nano Lett.* **2014**, *14*, 5068.
- [32] B. Z. Shakhshiri, *Chemical Demonstrations: A Handbook for Teachers of Chemistry*, Vol. 4, The University of Wisconsin Press, Madison, WI, USA, **1992**.
- [33] C. V. Thompson, *Annu. Rev. Mater. Sci.* **1990**, *20*, 245.
- [34] A. F. Mayadas, M. Shatzkes, *Phys. Rev. B* **1970**, *1*, 1382.
- [35] M. W. Rowell, M. D. McGehee, *Energy Environ. Sci.* **2011**, *4*, 131.